SERBIAN JOURNAL OF ELECTRICAL ENGINEERING
Vol. 12, No. 1, February 2015, 17-32

UDC: 621.313.333: 621.317.36 **DOI: 10.2298/SJEE1501017R**

Application of the Goertzel's Algorithm in the Airgap Mixed Eccentricity Fault Detection

Dejan Reljić[1], Josif Tomić[1], Željko Kanović[1]

Abstract: In this paper, a suitable method for the on-line detection of the airgap mixed eccentricity fault in a three-phase cage induction motor has been proposed. The method is based on a Motor Current Signature Analysis (MCSA) approach, a technique that is often used for an induction motor condition monitoring and fault diagnosis. It is based on the spectral analysis of the stator line current signal and the frequency identification of specific components, which are created as a result of motor faults. The most commonly used method for the current signal spectral analysis is based on the Fast Fourier transform (FFT). However, due to the complexity and memory demands, the FFT algorithm is not always suitable for real-time systems. Instead of the whole spectrum analysis, this paper suggests only the spectral analysis on the expected airgap fault frequencies employing the Goertzel's algorithm to predict the magnitude of these frequency components. The method is simple and can be implemented in real-time airgap mixed eccentricity monitoring systems without much computational effort. A low-cost data acquisition system, supported by the LabView software, has been used for the hardware and software implementation of the proposed method. The method has been validated by the laboratory experiments on both the line-connected and the inverter-fed three-phase four-pole cage induction motor operated at the rated frequency and under constant load at a few different values. In addition, the results of the proposed method have been verified through the motor's vibration signal analysis.

Keywords: Induction motor, Airgap mixed eccentricity, MCSA, Goertzel's algorithm.

1 Introduction

Three-phase cage induction motors are by far the most widely used rotating electrical machines in many industrial applications [1]. Their simple and robust construction, reliability, low cost and less maintenance are benefits that make them the right choice in industrial production systems. Developments in power electronics and digital control have led to the use of cage induction motors not only in low-performance drives, but also in high-performance applications.

[1]University of Novi Sad, Faculty of Technical Sciences, Trg Dositeja Obradovića 6, Novi Sad, Serbia; E-mails: reljic@uns.ac.rs, tomicj@uns.ac.rs, kanovic@uns.ac.rs

Even though cage induction motors are reliable, there are still problems with electrical and mechanical types of faults. The cage induction motor faults can cause the downtime of industrial processes and create production losses. Furthermore, they can also have a serious impact on the safety of people and environment (e.g. chemical industry). Hence, the early fault detection and the diagnosis of cage induction motors are of great importance. This enables repair actions to be planned before more serious damage occurs. Besides, early fault detection reduces maintenance costs.

The most common electrical faults of the cage induction motor include shorted and open turns on a stator phase winding, broken rotor bars, and broken rotor end-rings, while mechanical faults include airgap eccentricity (static, dynamic and mixed) and bearing failures [2 – 3]. The mechanical faults are prevalent and represent up to 60% of the faults [4]. Eccentricity fault represents up to 80% of the mechanical faults [4 – 5] and can be considered as a critical failure in an induction motor. Therefore, particular attention needs to be drawn to any signs of presence of eccentricity.

Due to the significance of early eccentricity fault detection, a large number of methods for induction machine condition monitoring and fault diagnosis have been proposed in the literature [2 – 13]. The methods are based on the mechanical vibration signals and motor current signal analysis in the steady-state and/or transient operation [2 – 13]. This is a non-intrusive way to test the induction motor. However, vibration sensors are expensive for industrial systems. On the other hand, stator currents can be easily measured via external inexpensive current sensors. Therefore, current-based methods have become the most common methods for the airgap eccentricity fault detection at an early stage.

The current-based method that has drawn researchers' attention is the motor current signature analysis (MCSA) [13]. This method is readily available, simple and cost-effective, and provides advantage over the techniques based on the measurement and analyses of motor vibration signals. Likewise, the method requires only one current sensor. MCSA technique is most often applied by monitoring and recording the motor line current, and then performing off-line digital signal processing of the recorded current signal by applying the Fast Fourier transform (FFT), which gives the current frequency spectrum. The spectrum is then analyzed, and the fault type is determined based on the characteristic current frequency components [2 – 4, 6 – 11, 13].

In this paper the MCSA method has been employed for the on-line airgap mixed eccentricity fault detection. Since the airgap mixed eccentricity problem can cause other faults in the induction motor [6], this fault should be detected at an early stage. Otherwise, the fault will propagate, leading to a more serious damage of the induction motor and the malfunction of an industrial system.

However, due to the complexity and memory demands, the MCSA method based on the FFT algorithm is not always suitable for real-time systems. Instead of the whole spectrum analysis, this paper suggests only the spectral analysis on the expected airgap mixed eccentricity fault frequencies employing the Goertzel's algorithm. This algorithm is simpler and numerically much more efficient than the FFT but only for a small number of frequency components of interest, which is the case here. Only the spectral analysis on the expected airgap mixed eccentricity fault frequencies is required. This reduces the expensive FFT hardware requirements (due to complex calculation and huge memory requirement). Hence, the on-line MCSA method can be implemented with low-cost hardware.

A low-cost data acquisition system, supported by the LabView software, has been used for the hardware and software implementation of the proposed MCSA method for the on-line detection of the airgap eccentricity based on the Goertzel's algorithm. The method has been validated by the laboratory experiments on both the line-connected and the inverter-fed three-phase four-pole cage induction motor operated at the rated frequency and under constant load at a few different values. Finally, results of the proposed method have been verified through the induction motor's vibration signal analysis.

2 Theoretical Background

2.1 Airgap eccentricity-related fault

Airgap eccentricity is a condition of unequal airgap that exists between the stator and the rotor [3, 10]. Airgap eccentricity can occur due to the misalignment of the stator and the rotor axes, ovality of the stator and/or the rotor bore, but it is often a side effect caused by faults in bearings or the shaft misalignment. Airgap eccentricity is also caused by mechanical problems in induction motor drives, such as shaft misalignment, or coupling misalignment in motor-load systems. The two main forms of airgap eccentricity are static and dynamic [3, 7, 10], while the presence of both types of eccentricity is called mixed eccentricity [14].

In the case of static eccentricity, the airgap length minima (maxima) position does not change with the rotor rotation [15]. Such type of eccentricity occurs if the rotor was not properly inserted into the stator bore or as a consequence of an oval-shaped stator magnetic circuit (Fig. 1). If the rotor is firmly tightened, the value of static eccentricity does not change during the motor operation [15]. Static airgap eccentricity creates a constant radial magnetic force, i.e. unbalanced magnetic pull (UMP), which acts on the rotor, trying to move it in the direction of the minima airgap, where magnetic reluctance is decreased [7]. The static eccentricity can lead to premature bearings failure.

Dynamic eccentricity occurs when the rotor axis does not align with the axis of rotation (Fig. 1). As a consequence, the airgap length minima (maxima) position rotates together with the rotor. Dynamic eccentricity occurs as a result of bearing wear or due to a bent shaft and creates a rotating UMP that affects the rotor and revolves with the rotor [7]. Dynamic eccentricity is dangerous, since its value changes during the motor operation and in some cases can lead the rotor to rub against the stator [15].

Finally, the presence of both types of eccentricity is called mixed eccentricity. In this condition, stator, rotor and rotational axes are displaced with respect to each other (Fig. 1). Since both static and dynamic eccentricities exist simultaneously in practice [14], only mixed eccentricity is considered in this paper.

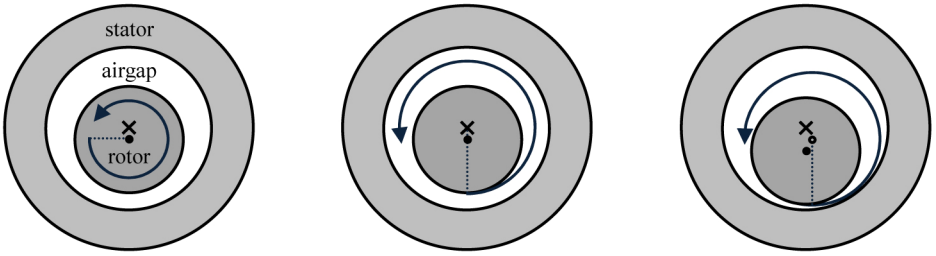

Fig. 1 – *Illustration of static (left), dynamic (middle) and mixed (right) airgap eccentricity of an induction motor.*

In practice, a certain amount of static and dynamic airgap eccentricity always exists, even in a healthy motor. The permissible limit of airgap eccentricity (radial) depends on the motor construction. It is considered that the permissible value of airgap eccentricity is 10% for a healthy motor [3, 7, 11]. On the other hand, motor manufacturers even try to reduce the eccentricity level below 10% in order to reduce the acoustic noise and motor vibrations [3, 7]. If airgap eccentricity value is not kept within the permissible level, potentially serious faults can occur, as previously stated. In high power induction motors, the eccentricity level above 25% can be considered dangerous [7].

2.2 Detection of airgap eccentricity

Traditionally, the MCSA method is used to detect abnormal level of airgap eccentricity [2 – 3, 11, 15]. This is a popular approach and the method has received many researchers' attention in recent years. The method relies on the fact that the mechanical airgap asymmetry causes a change in the airgap magnetic field, i.e. a change in the distribution of space harmonics in the airgap as well as the creation of additional frequency components in the stator current spectrum. Airgap eccentricity can be detected by monitoring particular

frequency components f_{ec} in the stator current spectrum [2 – 3, 10, 16] given by the following relationship:

$$f_{ec} = f_s \left[\left(nR \pm n_d \right) \frac{1-s}{P} \pm 2n_{sat} \pm \nu \right], \tag{1}$$

where f_s is the stator supply frequency, n is an integer (1,2,3…), R is the number of rotor slots, n_d is the eccentricity order (0 in the case of static eccentricity; 1,2,3… in the case of dynamic eccentricity), s is the slip, P is the number of pole pairs, n_{sat} models magnetic saturation (0, 1, 2…) and ν is the harmonic order of the stator supply voltage (1,3,5,7,…).

The equation (1) can be rearranged in the following way [16]:

$$f_{ec} = f_s \left[\left(nR \frac{1-s}{P} \pm \nu \right) \pm \left(n_d \frac{1-s}{P} \pm 2n_{sat} \right) \right]. \tag{2}$$

It can be seen from (2) that the terms in the first parentheses represent the rotor slot harmonics, i.e. the frequency components that occur as a consequence of static eccentricity are equal to the frequencies of the rotor slot harmonics. On the other hand, dynamic eccentricity creates additional frequency components around the rotor slot harmonics. Moreover, in the case of saturation, new frequency components around dynamic-eccentricity-characteristic components will occur [16].

The equations (1) and (2) can be used for the separate detection of static and dynamic airgap eccentricity, but under assumption that the motor construction, i.e. R and P, is well known. However, this is in general unknown to the user, making this approach impractical. Besides, characteristic frequency components from (1) and (2) are the function of the slip, so the change in the motor load will affect a certain change of the frequency spectrum. It means that, for a reliable assessment of eccentricity faults, the measuring of the slip (or the rotor speed) is desirable. This is not a problem in the speed-controlled induction motor drives, but it is a problem for the mains-fed motor drives. Furthermore, the existence of the rotor slot harmonics in (2) depends on the number of R and P combinations [17 – 18]. These components are presented in the frequency spectrum of the stator current if R satisfies the relationship (3) for the upper slot harmonic or (4) for the lower slot harmonics [17 – 18]:

$$R = 2P\left[3\left(m \pm q \right) \pm r \right], \tag{3}$$

$$R = 2P\left[3\left(m \pm q \right) \pm r \right] \pm z, \tag{4}$$

where r, z, m and q are real numbers that satisfy the following relations: $r = 0$ or $r = 1$, $z = 1$ or $z = 2$ and $m \pm q = 0,1,2,3,\ldots$ Likewise, it has been shown in [19] that the MCSA method based on (1) and (2) cannot be used to detect the

eccentricity-related fault signatures of static airgap eccentricity, as well as dynamic airgap eccentricity based on the lower sideband detection, because the variations in the sideband magnitudes between the healthy and faulty motors are small. These are certain drawbacks of the MCSA method for the airgap eccentricity fault detection approach based on (1) and (2).

In practice, static eccentricity and dynamic eccentricity exist simultaneously and are referred to as airgap mixed eccentricity [3, 14, 20]. Under airgap mixed eccentricity condition the stator current contains the following frequency components f_{mec} [3, 14, 20 – 22]:

$$f_{mec} = f_s \left[1 \pm k \frac{1-s}{P} \right] = f_s \pm k f_r \,, \tag{5}$$

where k is an integer (1,2,3,…) and f_r is the mechanical rotational frequency of the motor. For $k = 1$, the specific fault frequency components from (5) occur at $f_s - f_r$ (lower sideband) and $f_s + f_r$ (upper sideband). The variations in the magnitudes of these two sidebands between the healthy and faulty motors are, according to [21], over 20 dB. This is noticeable even when the motor operates at light load, which is the main benefit of this approach. The results presented in [21] also indicate the increase in the sidebands magnitude with the increase of the airgap eccentricity level, which makes it much easier to distinguish between the healthy and the faulty motors. Another important issue is that there is no mask effect in (5), since the eccentricity frequency is far enough from the supply frequency associated component [22].

The focus of this paper is airgap mixed eccentricity. Both sideband components (the lower and the upper sidebands) from (5) have been observed. It is obvious from (5) that both sidebands depend on the slip, i.e. motor load. Therefore, the change in the motor load will have a certain effect on the frequency spectrum shifting. However, for normal motor load values, the slip changes will not significantly affect the accuracy of the magnitude detection of sidebands. That means that the information on the slip, or the motor rotational speed, at normal load conditions is not essential. Instead, the proper frequency window should be set to enable an accurate identification of the eccentricity related components.

Although the MCSA method is a powerful technique for the airgap eccentricity fault detection, the eccentricity-related fault in induction motors can also be successfully detected using the vibration signal analysis [23 – 24]. The characteristic eccentricity-related frequency components f_{ecm} which exist in the motor vibration signals are [3, 24]:

$$f_{ecm} = 2 f_s \pm f_r \,. \tag{6}$$

The component at twice fundamental frequency from (6) indicates static eccentricity, while sidebands from (6) indicate dynamic eccentricity. An

increase in vibration level can be used to detect eccentricity fault. In this paper, these frequency components have been observed only as a confirmation of the eccentricity fault detection based on the MCSA method, i.e. (5).

3 MCSA Method Based on the Goertzel's Algorithm

The discrete Fourier transform (DFT) is the basic tool used for the MCSA. The DFT performs the Fourier transform of a discrete-time signal with N samples. However, the direct DFT computational complexity is $O(N^2)$ and for large series it can take a considerable amount of computation time [25]. A much faster algorithm has been developed by Tukey and Cooley [26], called the FFT. There are many variations of the FFT algorithms, but a radix-two decimation-in-time is by far the most widely used FFT algorithm. This algorithm reduces the number of computations from $O(N^2)$ to $O(N\log_2 N)$ [25 – 26]. Thus, the computation of the DFT becomes practical, particularly for large N. The only requirement is that N is restricted to be a power of 2 (radix-two).

Nevertheless, when a limited number of frequency components are needed to be computed, the Goertzel's algorithm [27] can be more efficient than the FFT based algorithms. The Goertzel's algorithm is a simple DFT. The first-order and the second-order Goertzel's algorithms are explained in [27]. The second-order Goertzel's algorithm is more efficient than the first-order Goertzel's algorithm [28]. The Goertzel's algorithm performs the DFT using an IIR filter calculation [28]. The z-domain transfer function of the second-order Goertzel filter is [27 – 30]:

$$H_K(z) = \frac{1 - \mathrm{e}^{-\mathrm{j}\frac{2\pi K}{N}} z^{-1}}{1 - 2\cos\left(\frac{2\pi K}{N}\right) z^{-1} + z^{-2}}, \tag{7}$$

where K is a coefficient for respective frequency components (Kth DFT component) in the input signal x of length N.

The respective difference equation of the above second-order IIR system is given by [30]:

$$y_K[n] = x[n] - x[n-1]\mathrm{e}^{-\mathrm{j}\frac{2\pi K}{N}} + 2\cos\left(\frac{2\pi K}{N}\right) y_K[n-1] - y_K[n-2], \tag{8}$$

where x represent a discrete input signal of length N ($n \in \mathbb{N}_0$), and y_K is its DFT, with zero initial conditions. Equation (8) can be described using the state variables [30]:

$$s[n] = x[n] + 2\cos\left(\frac{2\pi K}{N}\right) s[n-1] - s[n-2], \tag{9}$$

while the output is given by:

$$y_K[n] = X[K] = s[n] - \mathrm{e}^{-\mathrm{j}\frac{2\pi K}{N}} s[n-1], \tag{10}$$

with zero initial conditions.

The flow graph of the system is shown in Fig. 2. The left half of the graph contains a feedback (recursive) part and the right half contains a feedforward (nonrecursive) part. The feedback part is calculated at each iteration, while the feedforward part is calculated only after the last iteration [28]. For real data, the algorithm requires N real multiplication, $2N$ real additions, and a single complex multiplication with addition to compute the DFT value. For the computation of all N DFT values, the Goertzel's algorithm requires approximately N^2 real multiplications and $2N^2$ real additions. Thus, the computational complexity of the Goertzel's algorithm is $O(N^2)$ [31]. On the other hand, the direct application of the DFT requires N^2 complex multiplications and $N(N–1)$ complex additions, while the FFT requires $(N/2)\log_2 N$ complex multiplications and $N\log_2 N$ complex additions [31]. It is evident that the Goertzel's algorithm is more efficient than the direct DFT computation, but it is inefficient when compared with the FFT based algorithms. Nevertheless, in digital signal processing we do not always need to compute $X[K]$ from (10) at all N values of K, i.e. only a few frequency components are required rather than the entire spectrum. Namely, it has been shown that when calculating the DFT of the signal for only a few frequency components (M), this method is more efficient than the radix-2 FFT for $M < \log_2 N$ [29]. In this case the computational complexity of the Goertzel's algorithm is $O(MN)$. This is the main benefit of the Goertzel's algorithm. Moreover, the advantage of the Goertzel's approach over the radix-2 FFT algorithm is that N can be arbitrary (it does not have to be a power of 2) [30].

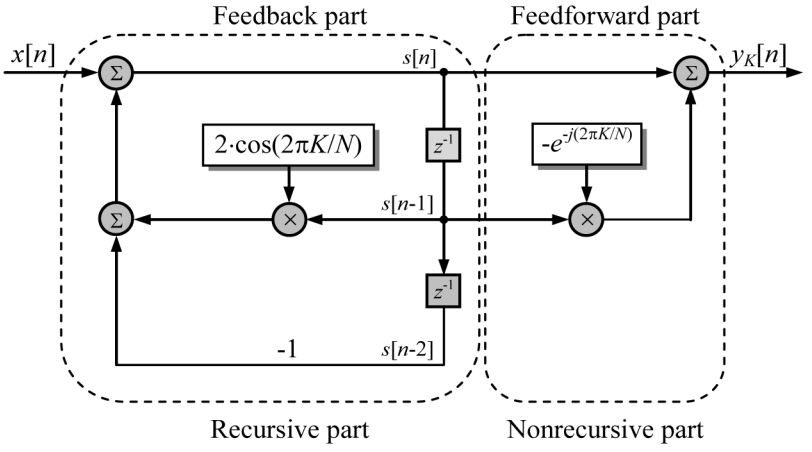

Fig. 2 – *Flow graph of the second-order Goertzel's algorithm.*

Since the Goertzel's algorithm processes samples in time order, it allows the calculation to begin when the first sample arrives. In contrast, the FFT must have the entire frame in order to start calculation [28]. Thus, the Goertzel's algorithm can be less demanding from the viewpoint of the memory capacity and it can perform at a very low latency [30]. In this paper, the Goertzel's algorithm has been efficiently applied for the on-line implementation of the MCSA technique for the airgap mixed eccentricity fault detection, i.e. for the detection of the current sidebands of interest according to (5).

4 Experimental Results

An experimental study was performed on the drive system from Fig. 3. The three-phase cage induction motor under test has the following rated data: 20 kW, 380 V, 40 A, 50 Hz, 1455 rpm. The induction motor can normally be connected to the sinusoidal three-phase supply (transfer switch in position 1), or can be supplied by the power inverter (transfer switch in position 2). Thus, two tests could be conducted: Test 1 – the motor was supplied from the three-phase mains, and Test 2 – the motor was supplied by the industrial power inverter. An optical encoder was attached to the shaft for speed measurement. A shaft-coupled wound-field synchronous generator with a resistive load bank was used to provide constant load conditions during experimental tests. During tests, the operational frequency of the induction motor was set to the rated value.

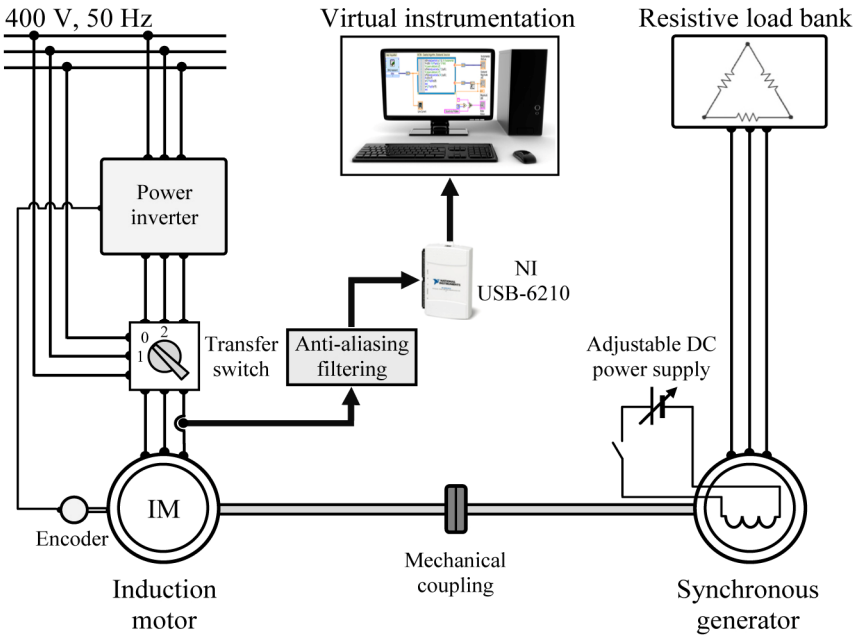

Fig. 3 – *Induction motor drive system configuration.*

The supply line current was sensed by a Hall-effect current clamp. The current signal from the clamp passed through an analog low-pass forth order Butterworth anti-aliasing filter with the cut-off frequency of 100 Hz, the stopband of 1.6 kHz, and the attenuation of –96 dB (the level of the noise floor). This provided an acceptably small amount of aliasing, which was especially important when the induction motor was supplied by the power inverter. Thus, a very high sampling rate of the data acquisition hardware was not mandatory. The filtered signal was then forwarded to the 16-bit A/D converter as a part of the NI USB-6210 data acquisition hardware [32]. In order to meet the Nyquist criterion, the sample rate was set to 3.2 kS/s, i.e. the oversampling technique was applied [33]. Since the rated speed of the induction motor is 1455 rpm and the supply frequency is 50 Hz, the mixed eccentricity frequency components from (5) for $k = 1$ (the lower and the upper sidebands) are in a 0.75 Hz wide window. Accordingly, the acquisition period was chosen to be 1 s. By using a rectangular window function, a 1 Hz spectral resolution is obtained. Since there is no mask effect (the eccentricity-related frequency components are far enough from other current frequency components), this enables the detection of the magnitudes of the mixed eccentricity-related frequency components with sufficient accuracy and a little motor speed variation. It should be mentioned that a certain error in magnitudes detection exists due to the reduced spectral resolution and spectral leakage. As the motor load increases, the error will increase. Nevertheless, since the variations in the magnitudes of the sidebands between the healthy and faulty motors are over 20 dB [21], quite accurate detection of their magnitudes is not mandatory, i.e. this error is negligible, especially for low-slip high-power induction motors. The experimental results reported below support this conclusion.

A monitoring system for the on-line airgap mixed eccentricity fault detection based on the MCSA method was realized in the LabVIEW software. LabVIEW program is called a virtual instrument (VI) [34]. It represents a shift from traditional hardware instrumentation to a software system which exploits the computing power. The magnitudes of the mixed eccentricity-related current frequency components (the lower and the upper sidebands from (5) for $k = 1$) and the fundamental frequency component (a total of three frequency components) were detected using the proposed Goertzel's algorithm. This was mplemented using the LabVIEW's Goertzel function in the MathScript RT Module. The VI developed for the airgap eccentricity fault monitoring system is shown in Fig. 4. Only the sideband component whose magnitude is closest to zero is considered as the eccentricity-related fault signature. The sideband magnitude for the healthy motor should be less than about –65 dB [17, 19, 35] and vice versa for the faulty motor. The frequency components with the higher values of k from (5) usually have much lower magnitudes. Hence, they were not considered as the eccentricity-related fault signatures.

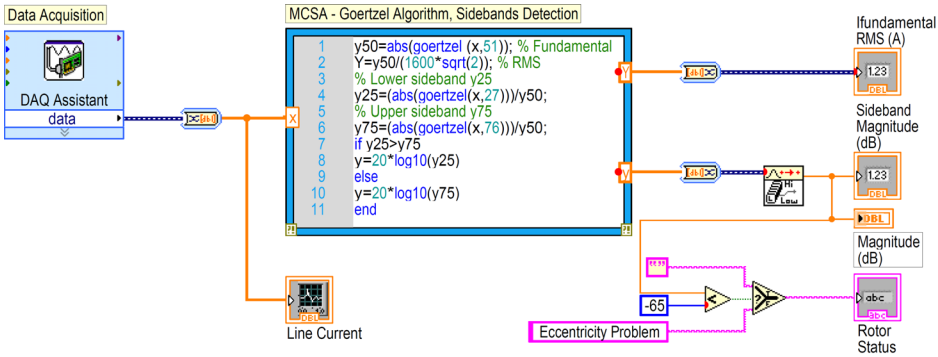

Fig. 4 – *LabVIEW VI block diagram of the airgap mixed eccentricity fault monitoring system.*

During tests, the wound-field synchronous generator with the resistive load bank was providing constant load conditions, as follows: no-load, 3 kW, 4 kW, 5 kW, and 6 kW. Unfortunately, the motor full-load torque could not be achieved due to the load bank limitations. As described earlier, two experimental tests were conducted: Test 1 – the induction motor was supplied from the three-phase mains, and Test 2 – the induction motor was supplied by the power inverter. In Test 2, the switching frequency of the power inverter was set to 8 kHz, while the induction motor was in constant *U*/*f* control. The tests provided the results presented in **Table 1**.

Table 1

Magnitude of the characteristic sideband component.

Test	Load [kW]	Rotor average speed [Hz]	Magnitude [dB]
Test 1	0	24.94	–39.0
Test 2	0		–38.5
Test 1	3	24.85	–39.3
Test 2	3		–37.6
Test 1	4	24.83	–39.5
Test 2	4		–37.8
Test 1	5	24.78	–40.0
Test 2	5		–37.7
Test 1	6	24.75	–40.6
Test 2	6		–37.6

The experimental results (**Table 1**) show that, independently of the power supply, the characteristic sideband magnitude is far above –65 dB. This indicates the presence of an abnormal level of the airgap mixed eccentricity. A certain differences in the magnitude of the characteristic sideband component between Test 1 and Test 2 (**Table 1**) are due to the applied voltage. In Test 1 the induction motor was supplied from the three-phase mains with a small voltage

asymmetry. Unsymmetrical voltages cause unsymmetrical currents. Thus, the magnitude of the airgap mixed eccentricity-related component varies per phases and will be different when compared with its value under symmetrical voltages. In Test 2 the induction motor was supplied by a pulse-width modulated (PWM) symmetrical voltage source. However, the PWM voltage source can cause motor torque and rotor speed pulsations due to the dead-time effect. This causes a certain error in the magnitude detection. Nevertheless, these effects did not significantly affect the fault diagnosis and the airgap mixed eccentricity fault was found to be very severe. It is noteworthy that the magnitude of the characteristic sideband component from **Table 1** is the average value during the diagnostic period of 10 s (Fig. 5). Observing Fig. 5, it is evident that the magnitude of the airgap mixed eccentricity-related component slightly changes over time. This could be caused by the rotor speed pulsation but also by the variation of the airgap eccentricity over time.

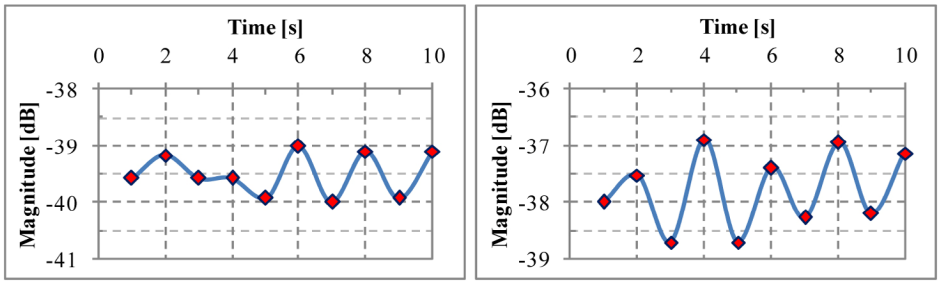

(a) (b)

Fig. 5 – (a) *Variation of the magnitude of the characteristic sideband component over time – illustration for Test 1.* (b) *Variation of the magnitude of the characteristic sideband component over time – illustration for Test 2.*

In order to validate the results obtained by the proposed MCSA method based on the Goertzel's algorithm, the off-line FFT analysis of the supply line current signal was also performed. Here, the acquisition period was set to 10 s, while the sample rate was not changed. By using a rectangular window function, a spectral resolution of 0.1 Hz was obtained. Therefore, much more accurate detection of the sidebands magnitude was expected (**Table 2**).

By comparing the results obtained with two different methods, the Goertzel's algorithm (**Table 1**) and the FFT (**Table 2**), it can be noticed that there is a little difference of the magnitude of the airgap mixed eccentricity-related component. These differences are decreasing at light load conditions. This is caused by the spectral resolution and spectral leakage. Still, this is acceptable. Illustration of the supply current spectra, performed by the FFT with the spectral resolution of 0.1 Hz, is shown in Fig. 6.

Table 2
Magnitude of the characteristic sideband component – FFT analysis.

Test	Load [kW]	Rotor average speed [Hz]	Magnitude [dB]
Test 1	0	24.94	–39.2
Test 2	0		–39.3
Test 1	3	24.85	–39.2
Test 2	3		–37.4
Test 1	4	24.83	–40.4
Test 2	4		–38.7
Test 1	5	24.78	–41.3
Test 2	5		–39.4
Test 1	6	24.75	–39.4
Test 2	6		–37.1

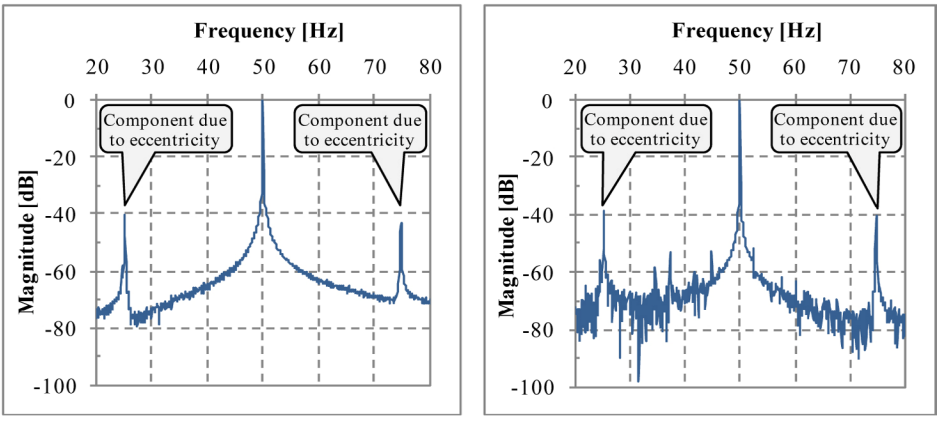

(a) (b)

Fig. 6 – (a) *Supply current spectra from the induction motor – illustration for Test 1.* (b) *Supply current spectra from the induction motor – illustration for Test 2.*

It should be pointed out that a very accurate frequency analysis (Fig. 6) is not desirable since it would lead to a huge time acquisition period in which the induction motor has to operate in a steady-state condition. This is inconvenient in industrial applications. Moreover, a huge acquisition time period would lead to the limitations of the hardware processing power.

To confirm the presence of eccentricity, evaluated by the MCSA method, the signal of vertical vibration at the drive side of the tested induction motor was also collected, using 100 mV/g accelerometers with the magnetic mounting and the NI USB-9234 acquisition card. Vibration signal was acquired with the sample rate of 25.6 kS/s, while the induction motor, supplied by the three-phase mains, was loaded for a period of 10 s by the synchronous generator with the

resistive load bank of 6 kW. The spectrum of the vertical vibration signal is shown in Fig. 7. It can be clearly distinguished that the vibration magnitudes are increased at 100 Hz, 75.25 Hz, and 124.75 Hz, which strongly points to the airgap eccentricity and confirms all previous results presented by the MCSA method. Moreover, it can also be noticed that the existence of one more peak is at 99.6 Hz. This frequency component is attributed to the presence of misalignment, which caused the airgap mixed eccentricity fault.

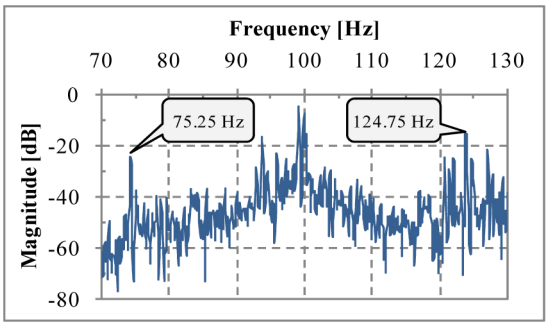

Fig. 7 – *Vertical vibration signal spectra of the induction motor.*

5 Conclusion

In this paper, the simple method for the on-line airgap mixed eccentricity fault detection of the induction motor was demonstrated. The method is based on the MCSA using the efficient Goertzel's algorithm instead of the FFT. The algorithm was employed for predicting the magnitudes of the characteristic airgap mixed eccentricity-related frequency components.

The effectiveness of the proposed method was demonstrated by experiments on both the line-connected and the inverter-fed induction motor. Satisfactory results were obtained. Moreover, the results of the proposed method were validated through the motor's vibration signal analysis.

6 Acknowledgment

This research was supported by the Ministry of Education, Science and Technological Development of the Republic of Serbia under project III42004.

7 References

[1] S. K. Bhattacharya: Electrical machines, 3rd edition, Tata McGraw-Hill Education, New Delhi, India, 2009.

[2] P. Vas: Parameter Estimation, Condition Monitoring, and Diagnosis of Electrical Machines, Clarendon Press, Oxford, United Kingdom, 1993.

[3] S. Nandi, H. A. Toliyat, X. Li: Condition Monitoring and Fault Diagnosis of Electrical Motors – A Review, IEEE Transactions on Energy Conversion, Vol. 20, No. 4, December 2005, pp. 719 – 729.

[4] J. Faiz, B. M. Ebrahimi, B. Akin, H. A. Toliyat: Comprehensive Eccentricity Fault Diagnosis in Induction Motors Using Finite Element Method, IEEE Transactions on Magnetics, Vol. 45, No. 3, March 2009, pp. 1764 – 1767.

[5] J. Faiz, B. M. Ebrahimi, M.B. B. Sharifian: Finite Element Transient Analysis of an On-Load Three-Phase Squirrel-Cage Induction Motor With Static Eccentricity, Journal of Electromagnetics, Vol. 27, Jun 2007, pp. 207 – 227.

[6] P. J. Tavner, J. Penman: Condition Monitoring of Electrical Machines, John Wiley and Sons, New York, USA, 1987.

[7] W. Thomson, R. Gilmore: Motor Current Signature Analysis to Detect Faults in Induction Motor Drives – Fundamentals, Data Interpretation and Industrial Case Histories, 32nd Turbomachinery Symposium, Houston, TX, USA, 2003, pp. 145 – 156.

[8] W.T. Thomson, M. Fenger: Current Signature Analysis to Detect Induction Motor Faults, IEEE Industry Applications Magazine, Vol. 7, No. 4, July/August 2001, pp. 26 – 34.

[9] M. El H. Benbouzid: A Review of Induction Motors Signature Analysis as a Medium for Faults Detection, IEEE Transactions on Industrial Electronics, Vol. 47, No. 5, October 2000, pp. 984 – 993.

[10] J.R. Cameron, W.T. Thomson, A.B. Dow: Vibration and Current Monitoring for Detecting Airgap Eccentricity in Large Induction Motors, IEE Proceedings B, Vol. 133, No. 3, May 1986, pp. 155 – 163.

[11] W. Thomson: On-Line Motor Current Signature Analysis Prevents Premature Failure of Large Induction Motor Drives, Maintenance and Asset Management, Vol. 24, No. 3, May/June 2009, pp. 30 – 35.

[12] H. Douglas, P. Pillay, A K Ziarani: A New Algorithm for Transient Motor Current Signature Analysis Using Wavelets, IEEE Transactions on Industry Applications, Vol. 4, No. 5, Sept.-Oct. 2004, pp. 1361 – 1368.

[13] G. B. Kliman, J. Stein: Methods of Motor Current Signature Analysis, Electric Machines and Power Systems, Vol. 20, No. 5, September 1992, pp. 463 – 474.

[14] S. Nandi, R. M. Bharadwaj, H. A. Toliyat: Performance Analysis of a Three-Phase Induction Motor Under Mixed Eccentricity Condition, IEEE Transactions on Energy Conversion, Vol. 17, No. 3, September 2002, pp. 392 – 399.

[15] A. Miletić: Diagnostic Methods and Criteria for Assessment of Induction Motor Electromechanical Condition, Ms. Thesis, Faculty of Electrical Engineering and Computing, University of Zagreb, Zagreb, Croatia, 2002.

[16] D. Morinigo-Sotelo, Member, L. A. Garcia-Escudero, O. Duque-Perez, M. Perez-Alonso: Practical Aspects of Mixed-Eccentricity Detection in PWM Voltage-Source-Inverter-Fed Induction Motors, IEEE Transactions on Industrial Electronics, Vol. 57, No. 1, January 2010, pp. 252 – 262.

[17] S. Nandi, H. A. Toliyat: Detection of Rotor Slot and Other Eccentricity Related Harmonics in a Three Phase Induction Motor with Different Rotor Cages, IEEE–PEDES Conference Proceedings, Perth, Australia, 1 – 3 December 1998, pp. 135 – 140.

[18] A. Ferrah, P. J. Hogben-Liang, K. J. Bradley, G. M. Asher, M. S. Woolfson: The Effect of Rotor Design of Sensorless Speed Estimation Using Rotor Slot Harmonics Identified by Adaptive Digital Filtering Using the Maximum Likelihood Approach, Industry Applications Conference, 32nd IAS Annual Meeting, IAS '97, New Orleans, USA, 5 – 9 October 1997, pp. 128 –135.

[19] R. Supangat: On-line Condition Monitoring and Detection of Stator and Rotor Faults in Induction Motors, Ph.D. dissertation, School of Electrical and Electronic Engineering, The University of Adelaide, Adelaide, Australia, 2008.

[20] X. Huang, T. G. Habetler: Detection of Mixed Air Gap Eccentricity in Closed-Loop Drive-Connected Induction Motors, 4th IEEE International Symposium on Diagnostics for Electric Machines, Power Electronics and Drives, Atlanta, GA, USA, 24 – 26 August 2003, pp. 312 – 316.

[21] A. Intesar: Investigation of Single and Multiple Faults Under Varying Load Conditions Using Multiple Sensor Types to Improve Condition Monitoring of Induction Machines, Ph.D. dissertation, School of Electrical and Electronic Engineering, The University of Adelaide, Adelaide, Australia, 2008.

[22] C. Marcelo, J. P. Fossatti and J. I. Terra: Fault Diagnosis of Induction Motors Based on FFT, Fourier Transform – Signal Processing, Dr Salih Salih (Ed.), InTech, 2012.

[23] J. Grieger, R. Supangat, N. Ertugrul, W. L. Soong, D. A. Gray, C. Hansen: Estimation of Static Eccentricity Severity in Induction Motors for On–Line Condition Monitoring, 41st IEEE Industry Applications Conference, Tampa, Florida, USA, 8 – 12 October 2006, pp. 2312 – 2319.

[24] D. G. Dorrell, W. T. Thomson, S. Roach: Analysis of Airgap Flux, Current and Vibration Signals as a Function of the Combination of Static and Dynamic Airgap Eccentricity in 3-Phase Induction Motors, IEEE Transactions on Industry Applications, Vol. 33, No. 1, Jan/Feb 1997, pp. 24 – 34.

[25] A. V. Oppenheim, R. W. Schafer, J. R. Buck: Discrete-Time Signal Processing, 2nd edition, Tsinghua University Press, Beijing, China, 2005.

[26] J. W. Cooley, J. W. Tukey: An Algorithm for the Machine Calculation of Complex Fourier Series, Mathematics of Computation, Vol. 19, 1965, pp. 297 – 301.

[27] G. Goertzel: An Algorithm for the Evaluation of Finite Trigonometric Series, American Mathematical Monthly, Vol. 65, No. 1, January 1958, pp. 34 – 35.

[28] R. Chassaing, D. Reay: Digital Signal Processing and Applications with the TMS320C6713 and TMS320C6416 DSK, 2nd ed., John Wiley and Sons, New Jersey, USA, 2008.

[29] J. G. Proakis, D. G. Manolakis: Introduction to Digital Signal Processing, Macmillan Publishing Company, New York, USA, 1988.

[30] P. Sysel, P. Rajmi: Goertzel Algorithm Generalized to Non-Integer Multiples of Fundamental Frequency, EURASIP Journal on Advances in Signal Processing, Vol. 2012, No. 1, 2012, pp. 1 – 8.

[31] B. P. Lathi, Roger A. Green: Essentials of Digital Signal Processing, Cambridge University Press, New York, USA, 2014.

[32] NI USB-621x User Manual, National Instruments, 2009.

[33] http://www.ni.com/pdf/manuals/371931f.pdf

[34] A. V. Oppenheim, R. W. Schafer, J. R. Buck: Discrete-Time Signal Processing, 2nd edition, Tsinghua University Press, Beijing, China, 2005.

[35] J. Jerome: Virtual Instrumentation Using LabVIEW, PHI Learning Pvt. Ltd., New Delhi, India, 2012.

[36] J. Faiz, B. M. Ebrahim: Static Eccentricity Fault Diagnosis in an Accelerating No-Load Three-Phase Saturated Squirrel-cage Induction Motor, Progress in Electromagnetics Research B, Vol. 10, 2008, pp. 35 – 54.